Appl Phys B (2011) 102: 789–794
DOI 10.1007/s00340-010-4213-5

Applied Physics B
Lasers and Optics

Short wavelength red-emitting AlGaInP-VECSEL exceeds 1.2 W continuous-wave output power

T. Schwarzbäck · M. Eichfelder · W.-M. Schulz · R. Roßbach · M. Jetter · P. Michler

Received: 10 May 2010 / Revised version: 20 July 2010 / Published online: 18 September 2010

Abstract We present a vertical external cavity surface-emitting laser system based on a multi-quantum-well structure with 20 compressively strained GaInP quantum wells for an operation wavelength of around 665 nm with a monolithic integrated distributed Bragg reflector. With the help of an intra-cavity diamond heatspreader the laser operates in continuous-wave mode. Operation with a TEM_{00} Gaussian beam profile and a beam propagation factor of $M^2 \leq 1.05$ is shown as well as a high resolution spectrum of the laser line, which shows the etalon effect of the diamond. The laser can be operated at a maximum output power exceeding 1.2 W with a slope efficiency of $\eta_{\text{diff}} = 18\%$. At maximum output power the wavelength of the laser resonance is at 670 nm, which is shortest reported until now at powers exceeding 1 W. By rotating a birefringent filter in an extended folded cavity arrangement a wavelength tuning of 21 nm was attained.

1 Introduction

Vertical external cavity surface-emitting lasers (VECSELs) [1] have emerged recently as an important category of power-scalable semiconductor lasers in a wide range of applications in biophotonics, television or projectors and spectroscopy. Here, VECSELs overcome the disadvantages of common high-power edge-emitting semiconductor lasers which often suffer from insufficient beam quality and catastrophic optical mirror damage. By using external cavities and optical pumping, VECSELs achieve high continuous-wave (cw) output power and near-diffraction-limited beam quality with a TEM_{00} Gaussian beam profile. This is shown for the UV, in the visible and in the near infrared spectral region [2] up to the mid IR-range (2.x µm with III–V VECSELs, >5 µm with IV–VI VECSELs) [3]. By investigating a direct pumping of the quantum well (QW), the heat load due to the quantum defect can be decreased [4]. To expand the adressable spectral range of VECSELs, recent work was focused on using quantum dots (QDs) as light emitting elements [5, 6]. Other investigations were done to gain electrically pumped VECSELs [7–9]. Additional research was concentrated on the generation of ultrashort pulses in the ps and fs regime using a VECSEL geometry [10], even with frequency doubling [11].

Considering the red spectral range, the first demonstration of an AlGaInP-VECSEL in pulsed operation at 660 nm was presented in 2002 [12]. First cw operation at 660 nm was attained with a pumping source at 630 nm [13] in 2003. With an intra-cavity diamond heatspreader a barrier pumped VECSEL in cw operation was achieved [14] 2005. High-power operation with 1.1 W output power in the red at 675 nm and a frequency doubled UV-VECSEL was realized one year later [15]. UV output power was also increased to 60 mW per laser beam [16].

In this paper, we present a modified VECSEL structure to achieve high output power exceeding 1.2 W at 670 nm, which is ∼5 nm shorter compared to previous reported work in literature at comparable output powers [15]. By integrating a cladding layer between the QW packages, wide range diffusion of the charge carriers should be prevented. The QWs themselves were embedded in barrier layers, where the highest absorption of the pump light takes place. First, de-

T. Schwarzbäck (✉) · M. Eichfelder · W.-M. Schulz · R. Roßbach · M. Jetter · P. Michler
Institut für Halbleiteroptik und Funktionelle Grenzflächen and Research Center SCoPE, University of Stuttgart, Allmandring 3, 70569 Stuttgart, Germany
e-mail: t.schwarzbaeck@ihfg.uni-stuttgart.de
Fax: +49-0711-68563866

sign of a VECSEL chip, as well as the epitaxial growth is shown in detail. Afterwards, the experimental setup and the results of the laser characterization are discussed.

2 Design and epitaxial growth

The VECSEL chip is built up of a gain providing section and a monolithic integrated distributed Bragg reflector (DBR) with a broadband reflectivity $R > 99.9\%$. The structures are deposited by metal-organic vapor-phase epitaxy (MOVPE) in an AIX-200 horizontal reactor setup with standard sources (trimethylgallium, trimethylindium, trimethylaluminum, arsine and phosphine) at low pressure of 100 mbar and a temperature of 750°C on (100) n^+-GaAs substrate misoriented 6° toward the $[111]_A$ direction. The gain region is built up of 5 groups consisting of 4 compressively strained GaInP QWs with a thickness of approximately 6 nm to achieve emission wavelengths below 670 nm. As barrier material for the QWs $((Al_{0.33}Ga_{0.67})_{0.51}In_{0.49})_{0.50}P_{0.50}$ (simplified as AlGaInP) is used. Each QW package is embedded in $Al_{0.55}Ga_{0.45}InP$ cladding layers in a resonant periodic gain (RPG) structure on top of the DBR with an AlAs heat spreading layer in between. The cladding layers serve as blocking layers to prevent a long-range diffusion of the charge carriers. For high gain from the active area, it is important to locate the active layers in the antinodes of the standing-wave of the electric field (see Fig. 1), which is called RPG [17, 18]. With the help of a simulation based on a transfer matrix method the thickness of the individual cladding layers are determined. The structure, which is non-resonantly pumped at 532 nm, does not allow lattice matched growth of a window nor a capping layer because of the absorption of the pump light within the available materials [2]. The DBR consists of 55 $\lambda/4$ pairs of $Al_{0.50}Ga_{0.50}As$/AlAs, which provide a calculated reflectivity of $R > 99.9\%$ with a central wavelength of ~666 nm (room temperature) at normal incidence and a stopband width of about 40 nm. These two DBR materials have a bandgap which is high enough to avoid absorption at the emission wavelength. For further wavelength-selective enhancement, the chip surface is also placed in an antinode of the electric field to generate a sub-cavity resonance [2]. So the main epitaxial difference to previous work in this field [12, 14, 15] is the separate confinement heterostructure of the active region. In Fig. 2, a scanning electron microscopy (SEM) cross section of the sample is displayed where the active region and a part of the DBR with the AlAs heat spreading layer in between is shown. The image with its quite high contrast confirms the good epitaxial growth of the structure. Although, the sum of all QWs would for sure exceed the critical thickness of the strained material, we have a smooth surface with a measured roughness of $rms = 1.5$ nm (rms: root mean square).

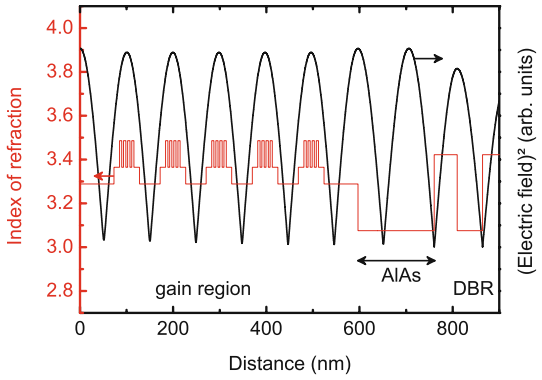

Fig. 1 Index of refraction and electric field intensity in a RPG VECSEL chip simulated with a transfer matrix method. The QW packages are located in the antinodes of the standing-wave of the electric field

Fig. 2 SEM cross section of the sample. In the upper part of the image the active region with the 5 QW packages (*brighter regions*) can be seen with the cladding layers (*darker regions*) surrounding them. In the *lower part* the DBR layer pairs are pictured. The *thick dark layer* in between is the AlAs heat spreading layer

This leads to the assumption that we have strain reducing in the structure. One strain releasing element would be the high number of interfaces in the structure. The strain reducing might also arise due to an unintentional slight misfit of the barrier or cladding composition. A sample with $5 \times 5\,mm^2$, which has an offset of ~4 nm between photoluminescence (PL) maximum (measured perpendicular to the sample surface) and cavity resonance (measured by reflection measurements) at room temperature, is cleaved from the wafer. This detuning δ (estimated $\delta = 9$ nm between gain and cavity resonance) is needed as a consequence of the generated heat in the structure due to the large quantum defect induced by the non-resonant pumping. The different temperature shifts of the gain and the cavity resonance reduce the detuning at elevated temperatures and enable

an effective operation of the laser. By bonding a 0.5 mm thick intra-cavity diamond heatspreader to the surface of the cleaved sample, heat transfer from the active region is improved to achieve cw operation. The type IIa single-crystal diamond from Element Six [19], which has a diameter of 4 mm with very low birefringence, is bonded with capillary forces [20]. No further post processing steps were done with the sample (neither substrate removal nor thinning).

3 Experimental setup

The laser chip, which is placed in a copper mount (see Fig. 3 for a schematic drawing) with an aperture for the pump and laser light, is actively cooled by a thermoelectric element (TEC) with an additional water/ethylene glycol cooling to reach heat sink temperatures of $T_{hs} = -31°C$. We use two different concave outcoupling mirrors with reflectivities of $R_{high} = 99.7\%$ and $R_{low} = 98.5\%$ at a wavelength of 660 nm and a radius of curvature of $R_c = 50$ mm, respectively. The cavity is adjusted to have a beam waist of about 77 µm on the VECSEL chip, which is the case for a resonator length of $L_{cavity} = 4.9$ cm. The structure is optically pumped by a commercially available frequency doubled Nd:YAG laser emitting at 532 nm and the pump beam is irradiated to the chip with an angle of about 40°. An image of the operating laser is shown in Fig. 4. The pump focusing lens has a focal length of 100 mm. By shifting the latter, the pump spot diameter can be varied. The pump focusing lens is adjusted to maximum output power at the emission wavelength.

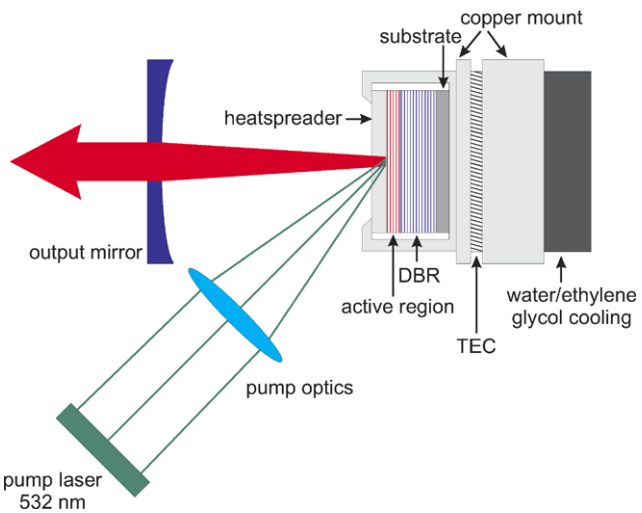

Fig. 3 Schematic drawing of the experimental setup of our VECSEL

4 Results

The emission characteristics are examined as a function of the irradiated pump power. A typical power transfer characteristic is displayed in Fig. 5 with a measured threshold of $P_{th} = 0.96$ W. The slope efficiency is $\eta_{diff} = 18\%$, which leads to a maximum output power exceeding 1.2 W. At highest output powers the wavelength is 670 nm, which is ~5 nm shorter than VECSELs with comparable output powers in literature [2]. In the GaInP/AlGaInP material system the confinement energy for the charge carriers signifi-

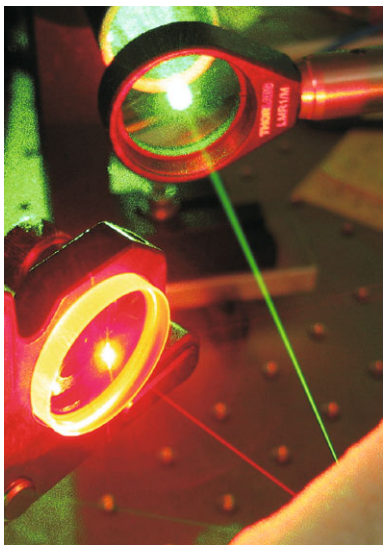

Fig. 4 Picture of the operating VECSEL taken with an 4 MP digital camera. No further post processing steps of the image were performed (except cropping). The green pump beam (some few Watts) and the red intra-cavity beam (some tens of Watts) are almost equal bright

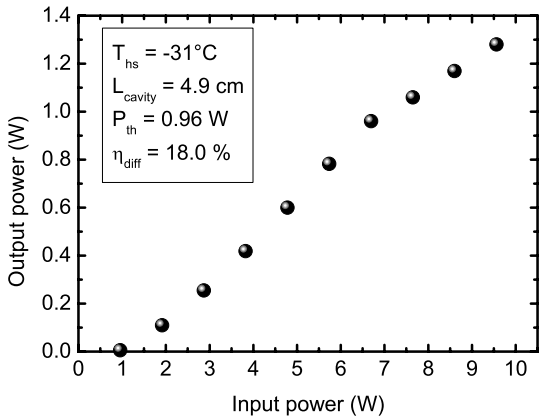

Fig. 5 Power transfer characteristics of the laser with output coupler reflectivity of $R_{low} = 98.5\%$. The copper mount temperature was $T_{hs} = -31°C$ and the cavity length was adjusted to $L_{cavity} = 4.9$ cm. The input power denotes the irradiated power on the sample neglecting reflection losses. A threshold power of $P_{th} = 0.96$ W and a slope efficiency of $\eta_{diff} = 18\%$ could be determined, which is labeled in the graph

cantly shrinks with decreasing the QW emission wavelength by every nanometer [21, 22]. Thus, shortening the emission wavelength results in a higher temperature sensitivity and therefore in lower output power. To reach high output powers at 670 nm the heat sink temperature has to be set to $T_{\mathrm{hs}} = -31\,^{\circ}\mathrm{C}$.

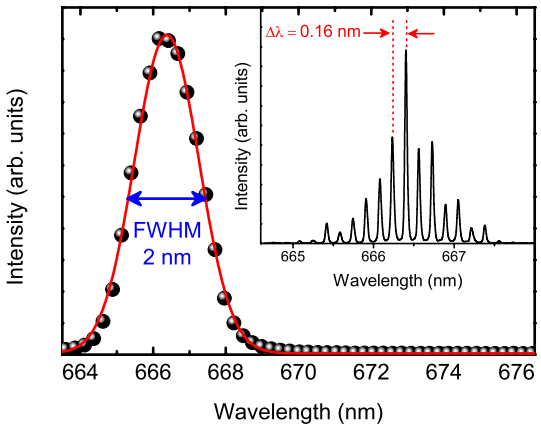

Fig. 6 Spectra of the laser emission (*dotted curve*) at moderate input powers of $P_{in} = 5.3\,\mathrm{W}$ with $R_{\mathrm{high}} = 99.7\%$ output coupler with fitted Gaussian function (*solid curve*). *Inset*: High resolution spectrum with $R_{\mathrm{low}} = 98.5\%$ output coupler measured with a Laser spectrum Analyser from HighFinesse GmbH [23]

In Fig. 6 a spectrum of the laser emission with an resolution of the spectrometer of about $\delta\lambda = 1\,\mathrm{nm}$ is shown. The laser resonance is centered at a wavelength of 666 nm with a full width at half maximum (FWHM) of FWHM = 2.0 nm. The inset shows a high resolution ($\delta\lambda = 15\,\mathrm{pm}$) scan of the spectrum measured with a multi-mode fiber-coupled Laser spectrum Analyser from HighFinesse GmbH [23]. Here, the Fabry–Pérot oscillations created by the intra-cavity diamond platelet can be seen. The FWHM of a single peak could be extracted to 36 pm. With help of the refractive index of diamond for the specific wavelength ($n = 2.41$) and the spectral separation distance of the oscillation maxima ($\Delta\lambda = 0.16\,\mathrm{nm}$), the thickness of the diamond can be calculated to approximately 560 µm.

As mentioned above, one of the superior characteristics of the VECSEL is the beam profile. Figure 7 illustrates the measured beam shape by a CMOS camera chip and its cross sections. The beam profile has a circular symmetric intensity distribution. The interference pattern is a measurement artifact which arises due to dust particles in the lower right section on the camera's attenuator. The cross sections in Fig. 7(b) and (c) show good accordance to the fits with a Gaussian function and confirm the good quality of the TEM_{00} Gaussian beam profile. However, highest laser output power is associated with appearance of higher order transverse modes [24].

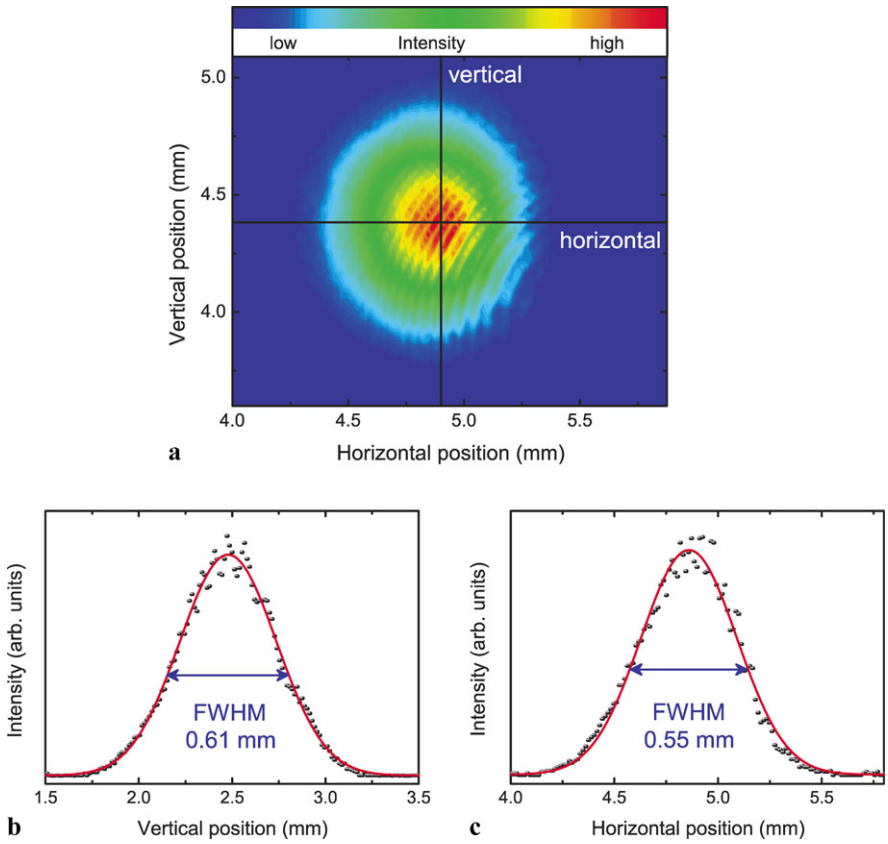

Fig. 7 (**a**) Typical beam profile of the laser at moderate input powers measured with a CMOS camera and its cross sections (*points*) in vertical (**b**) and horizontal (**c**) direction with fitted Gaussian functions (*solid curves*). The laser was operating with $R_{\mathrm{high}} = 99.7\%$ output coupler at an input power of $P_{\mathrm{in}} = 3.3\,\mathrm{W}$

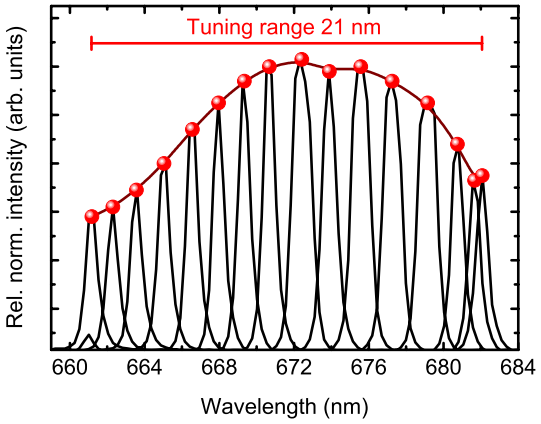

Fig. 8 Laser spectra measured during wavelength tuning

To determine the beam propagation factor M^2, a beam waist of the laser beam was generated by a biconvex lens with a focal length of $f = 300$ mm. The diameter, which is defined by the method of the second moment [25], was measured with the above mentioned CMOS camera 50 cm along the beam propagation axis starting at the location of the beam waist. The step size was chosen to be 2.5 cm to gain a reliable measurement with enough data in the range of the Rayleigh length and also more far away from the beam waist position. With this method the beam propagation factor of the laser with an output coupler reflectivity of $R_{\text{high}} = 99.7\%$ was measured to be $M^2 \leq 1.05$ at moderate input powers, which is close to an ideal Gaussian beam indicating a near-diffraction-limited beam and single-transverse-mode operation.

By changing the cavity design to an extended folded cavity in a 4 mirror z-type resonator configuration (3 external mirrors with a total cavity length of $L_{\text{cav}} = 486$ mm), it was possible to place a birefringent filter at Brewster's angle inside a fold of the cavity. Rotating the 2 mm thick filter around the normal axis of the surface enables us to tune the wavelength of the laser emission as can be seen in Fig. 8. The optical output of the different emission wavelengths is normalized to the emission at 672 nm. The optical output power at this measurement was 12.3 mW. The wavelength can be tuned within a range of 21 nm from 661 nm to 682 nm, respectively.

5 Conclusion

We have demonstrated a cw red VECSEL system emitting at around 665 nm operating with an intra-cavity diamond heatspreader. The output power of the laser exceeds 1.2 W with a wavelength of 670 nm. Furthermore, we have proven the expected good circular TEM_{00} beam quality in a near-diffraction-limited beam. Within an extended z-cavity and an additional birefringent element, a wavelength tuning range of 21 nm around a center wavelength of 672 nm was achieved.

To further increase the output power or to provide higher heatsink temperatures, a bigger detuning of gain maximum and cavity resonance could be preferable. Another way to optimize the structure is the RPG layout. A layout with 10 times 2 QWs per antinode could possibly provide the smaller amount of QWs per antinode with more charge carriers because of the therefore larger barrier or cladding layers surrounding them.

The next step would be to implement an additional nonlinear element (e.g. BBO frequency doubling crystal) in the extended cavity for frequency doubling, to fabricate a high-power cw UV laser source. By implementing InP/AlGaInP-QDs as active material, the spectral coverage and the tunability of the VECSEL could be extended [6, 26].

Acknowledgements The authors would like to thank E. Kohler for technical assistance with the MOVPE system.

References

1. M. Kuznetsov, F. Hakimi, R. Sprague, A. Mooradian, Technol. Lett. **9**, 1063 (1997)
2. S. Calvez, J.E. Hastie, M. Guina, O.G. Okhotnikov, M.D. Dawson, Laser Photonics Rev. **3**, 407 (2009)
3. N. Schulz, J.-M. Hopkins, M. Rattunde, D. Burns, J. Wagner, Laser Photonics Rev. **2**, 160 (2008)
4. S.-S. Beyertt, T. Kübler, U. Brauch, A. Giesen, E. Gerster, F. Rinaldi, P. Unger, OSA Trends Opt. Photonics **98**, 294 (2005)
5. T.D. Germann, A. Strittmatter, J. Pohl, U.W. Pohl, D. Bimberg, J. Rautiainen, M. Guina, O.G. Okhotnikov, Appl. Phys. Lett. **93**, 051104 (2008)
6. P.J. Schlosser, J.E. Hastie, S. Calvez, A.B. Krysa, M.D. Dawson, Opt. Express **17**, 21782 (2009)
7. M.E. Kurdi, S. Bouchoule, A. Bousseksou, I. Sagnes, A. Plais, M. Strassner, C. Symonds, A. Garnache, J. Jacquet, Electron. Lett. **40**, 671 (2004)
8. A. Bousseksou, S. Bouchoule, M. Kurdi, M. Strassner, I. Sagnes, P. Crozat, J. Jacquet, Opt. Quantum Electron. **38**, 1269 (2006)
9. P. Kreuter, B. Witzigmann, D.J.H.C. Maas, Y. Barbarin, T. Südmeyer, U. Keller, Appl. Phys. B, Lasers Opt. **91**, 257 (2008)
10. U. Keller, T. Südmeyer, Opt. Photonik **4**, 39 (2008)
11. O. Casel, D. Woll, M.A. Tremont, H. Fuchs, R. Wallenstein, E. Gerster, P. Unger, M. Zorn, M. Weyers, Appl. Phys. B, Lasers Opt. **81**, 443 (2005)
12. M.I. Müller, N. Linder, C. Karnutsch, W. Schmid, K.P. Streubel, J. Luft, S.-S. Beyertt, A. Giesen, G.H. Döhler, Proc. SPIE **4649**, 465 (2002)
13. M.I. Müller, C. Karnutsch, J. Luft, W. Schmid, K. Streubel, N. Linder, S.-S. Beyertt, U. Brauch, A. Giesen, G.H. Döhler, in *29th International Symposium on Compound Semiconductors*, vol. 174, ed. by M. Ilegems, G. Weimann, J. Wagner (IOP, Lausanne, 2003), p. 427
14. J.E. Hastie, S. Calvez, M. Dawson, T. Leinonen, A. Laakso, J. Lyytikäinen, M. Pessa, Opt. Express **13**, 77 (2005)
15. L.G. Morton, J.E. Hastie, M.D. Dawson, A.B. Krysa, J.S. Roberts, in *Conference on Lasers and Electro-Optics, 2006 and 2006 Quantum Electronics and Laser Science Conference (CLEO/QELS)* (2006), p. 1

16. J.E. Hastie, L.G. Morton, A.J. Kemp, M.D. Dawson, A.B. Krysa, J.S. Roberts, Appl. Phys. Lett. **89**, 061114 (2006)
17. M.Y.A. Raja, S.R.J. Brueck, M. Osinski, C.F. Schaus, J.G. McInerney, T.M. Brennan, B.E. Hammons, IEEE J. Quantum Electron. **25**, 1500 (1989)
18. S.W. Corzine, R.S. Geels, J.W. Scott, R.-H. Yan, L.A. Coldren, IEEE J. Quantum Electron. **25**, 1513 (1989)
19. Element Six Ltd., http://www.e6cvd.com
20. Z.L. Liau, Appl. Phys. Lett. **77**, 651 (2000)
21. P. Savolainen, M. Toivonen, M. Pessa, M. Corvini, M. Jansen, R.F. Nabiev, Semicond. Sci. Technol. **14**, 425 (1999)
22. J.-R. Dong, J.-H. Teng, S.-J. Chua, B.-C. Foo, Y.-J. Wang, L.-W. Zhang, H.-R. Yuan, S. Yuan, J. Appl. Phys. **95**, 5252 (2004)
23. HighFinesse GmbH, http://www.highfinesse.com
24. M. Kuznetsov, F. Hakimi, R. Sprague, A. Mooradian, IEEE J. Sel. Top. Quantum Electron. **5**, 561 (1999)
25. A.E. Siegman, in *Solid State Lasers: New Developments and Applications*, ed. by M. Inguscio, R. Wallenstein (Plenum, New York, 1993)
26. M. Eichfelder, W.-M. Schulz, M. Reischle, M. Wiesner, R. Roßbach, M. Jetter, P. Michler, Appl. Phys. Lett. **95**, 131107 (2009)